A Method for Determining the Sensor Degradation Rates of NOAA AVHRR Channels 1 and 2

A. WU AND Q. ZHONG

Lanzhou Institute of Plateau Atmospheric Physics, The Chinese Academy of Sciences, Lanzhou, People's Republic of China

21 August 1992 and 21 January 1993

ABSTRACT

A method is described to determine the degradation rates of NOAA Advanced Very High Resolution Radiometer (AVHRR) visible channels. Thirty-eight desert targets (each 20 km × 20 km) were selected over the northwest region of China after testing uniformity of the underlying surface. Two cloud-free datasets for the same satellite were sampled from two different periods several years apart. The functional relationships were established between the observed reflectances and the satellite observation angles. By allowing comparison of the functional relationships of the two different periods and computation of the sensor degradation rates using the stepwise method, the degradation rates were determined to be 5.8% and 4.6% per year for channels 1 and 2, respectively, based on the *NOAA-9* AVHRR data for October 1985 and September 1988.

1. Introduction

Satellites are the ideal tools for monitoring climate and environment changes because of the global extent and long time scale of their observations. Precise radiation measurements from satellites are required in order to extract the weak signal of climate variation. However, satellite radiometers often degraded at alarming rates when exposed to the harsh space environment, and onboard calibration systems were added to some instruments to maintain their standards over time. But unfortunately, the visible channels (channels 1 and 2) of the Advanced Very High Resolution Radiometer (AVHRR) flown on the existing National Oceanic and Atmospheric Administration (NOAA) polar orbiters had no onboard calibration capability. Therefore, some methodologies were developed using the earth's surface as a target to monitor the radiometric degradation over time. Many deserts are large, temporally stable and uniform, have high albedos and clear skies, and generally provide ideal natural targets for long-term, in-flight calibration of satellite radiometers.

Recent research [Staylor (1990) and Brest et al. (1992)] revealed the degradation rate of *NOAA-9* AVHRR channel 1 by selecting a large desert site as a natural earth target and comparing the monthly history observations. However, these studies need a large amount of long-term observation data and much computing time (Holben et al. 1990). Kaufman and Holben (1992) have developed an in-flight calibration for *NOAA-11* observations. More research is still needed in this area.

In this study, a method is presented to determine the degradation rates of *NOAA-9* AVHRR channels 1 and 2. This method requires relatively limited data for determining the degradation rates. This method consists of the following four steps.

1) Select a group of desert areas (about 20-km × 20-km scale for each area) as the targets in the northwest of China.

2) Eliminate the contamination of cloud for the collected datasets by thresholding on channels 1 and 4.

3) Sample the bidirectional reflectance data with different satellite viewing angles but with approximately the same solar zenith angles and establish the functional relationships between the observed reflectances and the satellite zenith angles for the two different periods.

4) Determine the degradation rates using the stepwise method by comparing the functional relationships of the two different periods.

The *NOAA-9* AVHRR LAC (local area coverage) data for October 1985 and September 1988 were used to determine the degradation rates of channels 1 and 2. After site selection, the available data were selected from 30/31 October 1985 and 4/5 September 1988 passes. During these days, most northwestern regions of China were cloud free and there were no precipitation processes before these days. For convenience, we define the data for 30/31 October 1985 as dataset A and the data for 4/5 September 1988 as dataset B. Owing to the delay of the crossing time, we choose dataset B, which is two months earlier than dataset A,

Corresponding author address: Prof. Q. Zhong, Lanzhou Institute of Plateau Atmospheric Physics, Chinese Academy of Sciences, Lanzhou, Gansu, 730000, People's Republic of China.

so that the solar zenith angles are approximately the same for both datasets.

2. Site selection and data editing

Deserts are not totally uniform, and therefore, the present search for the desirable desert sites is restricted to a group of small desert subregions that are more uniform. The Taklama and Badain Jaran Deserts, located at inland basins deep in the Asian continent where ocean moisture can hardly reach and the climate is extremely dry, are the largest and the third-largest deserts in the northwest of China, respectively. According to some spot investigations (Yang 1990; Gao 1989), surface vegetation is quite sparse and most of the desert regions are identically dominated by bare and dense dune bodies. Based on the high-resolution pictures from Landsat and the soil map in the northwest of China, it is not difficult to find such uniform desert subregions in the high-resolution pictures in the Taklama and Badain Jaran Deserts. Thirty-eight such uniform desert subregions are selected and their locations are listed in Table 1. Each consisted of AVHRR pixels from a 15′ × 10′ subregion, which is about 20 km × 20 km (approximately 350 pixels under nadir).

The *NOAA-9* AVHRR data for October 1985 were used for testing the uniformity of the subregions selected. Each subregion standard deviation of the albedo of the channel 1, $\sigma\alpha_1$, was usually smaller than 0.005 for clear days. Subregion-averaged albedos for both channels 1 and 2 decreased linearly with cosine of satellite zenith angle within the limited angular range (see Fig. 1), which indicates a degree of uniformity among all 38 subregions.

Considering that clouds may be present over the subregions, editing procedures are required to eliminate cloud cases. Here, the data of each subregion were edited independently for clouds. The editing was done in two steps.

1) Contamination by clouds usually does not occur in a uniform manner. Therefore, $\sigma\alpha_1$ should provide a relative means for determining whether the clouds may be present. Analyses indicated that the sample would be contaminated by clouds for $\sigma\alpha_1 > 0.01$. There, $\sigma\alpha_1 = 0.009$ was used as an editing threshold.

2) There were some concerns that thin cirrus clouds could cover some subregions and go undetected by step 1. Consequently, the subregion-averaged brightness temperature of channel 4, T_4, was used as a second editing parameter. The maximum subregion brightness temperatures T_{max} were obtained for each subregion, and the subregions would be edited for T_4 values 5°C or more below their T_{max}.

3. Monitoring of the degradation rates of AVHRR visible channels

Observed albedos (bidirectional reflectances) of AVHRR channels 1 and 2, even when the underlying surface is uniform, are functions of the satellite zenith angle, solar zenith angle, and azimuth angle. We must monitor the sensor's degradation under the same viewing geometry conditions, which means to monitor observed albedos under the same satellite zenith angle, solar zenith, and azimuth angle. The satellite zenith angle and azimuth angle for each subregion could be calculated (Wu 1990) with the orbital elements extracted from AVHRR 1b data. Table 2 lists angular parameter ranges for the entire dataset. It shows that there is an obvious difference in the azimuth angles between datasets A and B. Concerning the solar zenith angle, dataset B was obtained during early September, about two months earlier in the year than dataset A, but its equatorial crossing time was about 1 h later. Therefore, the range of the solar zenith angle values for set B is similar to that for set A. According to the bidirectional reflectance model used to characterize clear desert (Taylor and Stowe 1984), the variability of the reflectance pattern did not change greatly in such

TABLE 1. Locations of 38 desert target subregions.

	Latitude (N)	Longitude (E)
1	38°15′	78°15′
2	37°40′	79°00′
3	38°15′	79°30′
4	39°45′	79°45′
5	39°45′	80°15′
6	37°30′	80°45′
7	38°15′	81°05′
8	39°05′	81°15′
9	40°00′	81°30′
10	40°15′	82°00′
11	40°15′	82°35′
12	38°30′	82°40′
13	39°15′	82°45′
14	38°40′	83°45′
15	39°50′	84°40′
16	40°15′	84°45′
17	39°10′	85°00′
18	37°50′	85°45′
19	40°30′	86°00′
20	39°10′	86°10′
21	40°20′	86°30′
22	40°15′	87°45′
23	39°48′	89°00′
24	40°15′	89°00′
25	40°18′	89°15′
26	39°35′	90°45′
27	39°35′	91°20′
28	40°10′	94°10′
29	40°45′	95°45′
30	40°15′	100°45′
31	40°15′	101°45′
32	40°30′	102°30′
33	38°00′	103°30′
34	37°40′	104°10′
35	39°05′	104°40′
36	39°40′	106°10′
37	40°00′	106°20′
38	40°30′	108°10′

TABLE 2. Angular parameter ranges for datasets A and B.

Dataset	Data time	Solar zenith	Satellite zenith	Azimuth	
				Forward	Backward
A	30 October 1985	56°–67°	3°–56°	135°–136°	44°–45°
	31 October 1985	56°–68°	0°–61°	134°–137°	43°–46°
B	4 September 1988	49°–68°	8°–61°	169°–172°	8°–11°
	5 September 1988	48°–67°	5°–63°	169°–172°	9°–11°

limited solar zenith angle range. Therefore, if we assume such pattern behavior is also similar to that of our desert subregions, observed albedo in both channels is mainly associated with the satellite zenith angle and azimuth angle after we chose the data with the limited solar zenith angle ranging between 50° and 65°. Considering that there are differences in azimuth angles between the two periods (as seen in Table 2) that would cause systematic errors due to the anisotropy, we azimuthally corrected dataset B to that of dataset A by introducing the anisotropic factor for deserts (Staylor and Suttles 1986). Dataset B is multiplied by a factor, $F(\theta_0, \theta, \psi_1)/F(\theta_0, \theta, \psi_2)$, where $F(\theta_0, \theta, \psi_j)$ $(j = 1, 2)$ are anisotropic factors for dataset A $(j = 1)$ and B $(j = 2)$, respectively; θ_0 is the averaged solar zenith angle; θ is the satellite zenith angle; and ψ_j is the azimuth angle. After the above correction, dataset B can be assumed to have the same azimuth angle as dataset A, and its value is constant at about 135° (forward reflectance) or about 45° (backward reflectance). We use only the forward-reflectance data in our analysis because more samples are available.

After the normalization of azimuth angle, observed albedos α_i $(i = 1, 2)$ of AVHRR channels 1 and 2 versus $\cos\theta$ are illustrated in Figs. 1 and 2, respectively, for datasets A and B. Although observed albedos for both datasets and channels decrease linearly with $\cos\theta$ linearly, the values of dataset B are below those of dataset A, indicating that sensor degradations have occurred for both channels 1 and 2.

To determine the degradations of both channels between the two periods, degradation factors D_i $(i = 1$ for channel 1 and $i = 2$ for channel 2) were introduced to correct α_i as

$$\alpha_i' = D_i\alpha_i \quad i = 1, 2; \tag{1}$$

D_i was always set equal to 1.0 for dataset A. For dataset B in 1988, we also set the initial value of D_i equal to 1.0. Then, α_i' can be obtained from (1), and we can derive the linear regression equation of α_i' versus cosine of satellite zenith angle $\mu = \cos\theta$ by the least-squares method with the entire sample of data from sets A and B:

$$\hat{\alpha}_i = a_{0i} + a_{1i}\mu. \tag{2}$$

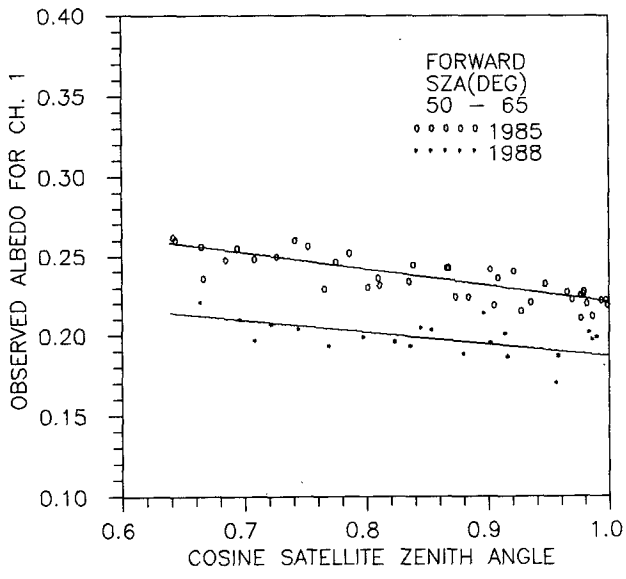

FIG. 1. Observed albedo for channel 1 versus cosine satellite zenith angle.

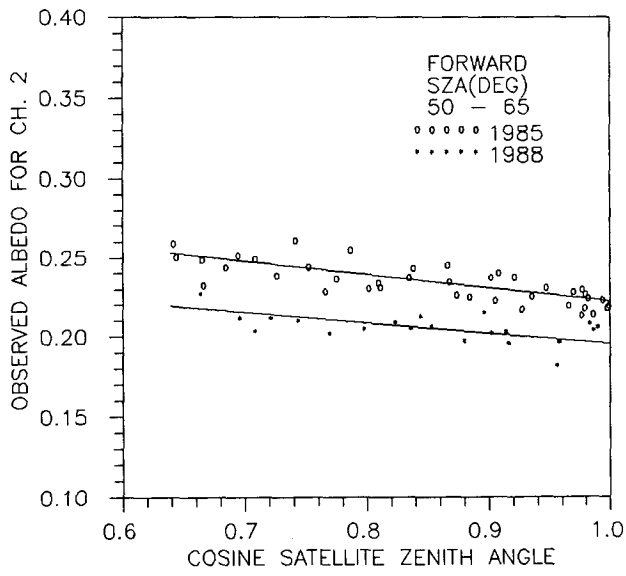

FIG. 2. As Fig. 1 but for channel 2 only.

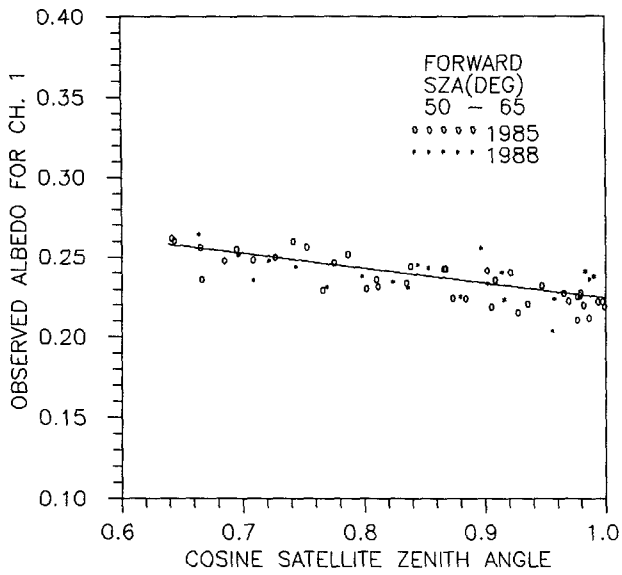

FIG. 3. As Fig. 1 but with the degradation correction.

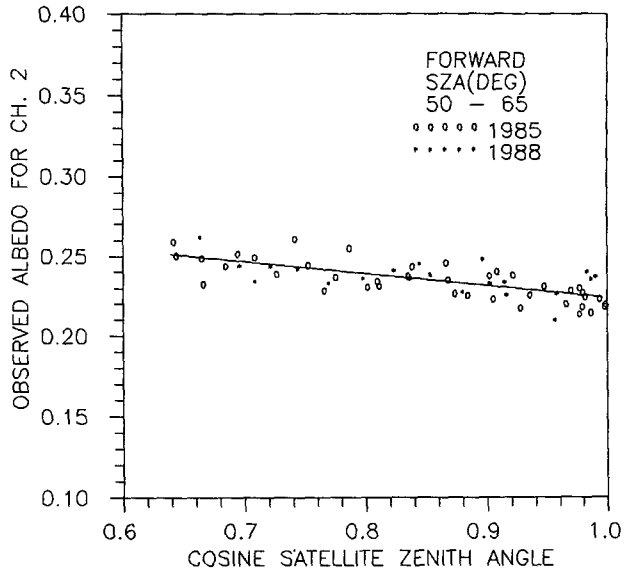

FIG. 4. As Fig. 2 but with the degradation correction.

This new regression was used to compute D_i as

$$D_i = \frac{\hat{\alpha}_i}{\alpha_i}, \tag{3}$$

and a new value of D_i for dataset B was determined. After iteration, an averaged near-minimal standard deviation, $\sigma\alpha_i'$, was obtained, and the results of channels 1 and 2 are shown in Figs. 3 and 4, respectively. After degradation corrections were made, it can be seen that good agreement exists for the albedos for the two periods. The degradation values for both channels 1 and 2 of *NOAA-9* between the two periods are listed in Table 3. Compared to the work of Staylor (1990), in which the degradation rate of the *NOAA-9* AVHRR channel 1 sensor was estimated to be 6% per year, our result (5.8% for channel 1) is in good agreement. Here, an assumption of linear degradation is adopted between the two periods for both channels 1 and 2. More annual data must be collected to investigate the channel's actual degradations, which may be not linear.

Channel 2 is sensitive to water vapor amount in the atmosphere, and therefore, its measurements would include the noise caused by water vapor amount. According to climatological records of the water vapor amount at Dunhuang (40°8′N, 94°47′E), the water vapor amounts are 1.3 cm for September and 1.0 cm for October, respectively. Our study (Wu and Zhong 1992) indicated that the values of ratio vegetation index α_2/α_1 in the edge of the Badain Jaran Desert change from 0.94 in summer to 1.00 in winter. This shows that water vapor amount really does have an effect on channel 2. Since the season of dataset A (October) is close to that of dataset B (September), the present method has no consideration of the effect of water vapor on channel 2.

For a desert area, the ratio α_2/α_1 is a stable parameter that depends on the inherent radiative property of the desert. These characteristics could be used to validate the degradation rate of 4.6% for channel 2. After the observed albedos of channels 1 and 2 of dataset B have been corrected with degradation rates 5.8% and 4.6%, respectively, the averaged ratio α_2/α_1 of dataset B (1.01) is very close to that of dataset A (1.00). This result indicates the reliability of the degradation rate of channel 2 obtained in this paper.

This study analyzes only desert scene types that have spectrum wavelengths longer than most other scene types such as cloud, snow, vegetation, etc. Staylor (1990) discussed whether the sensor degradations determined for desert scene types are applicable to other scene types. According to his study, he believes that the sensor degradations are essentially uniform across the response bandwidth and that the degradation rates determined for desert targets are applicable to all scene types.

4. Summary and discussion

Thirty-eight desert subregions (each 20 km × 20 km) were selected as the target sites to monitor the

TABLE 3. Degradation values for *NOAA-9* visible channels from October 1985 to September 1988.

	Degradation factor	Degradation rate (%)	Yearly averaged degradation rate (%)
Channel 1	1.19	16.3	5.8
Channel 2	1.15	13.0	4.6

radiometric degradation of the visible channels (channels 1 and 2) of *NOAA-9* AVHRR between the two different periods (October 1985 and September 1988). After being edited for clouds, the data were sampled as a function of satellite zenith angle, which revealed that *NOAA-9* visible channel sensors had incurred substantial degradation between the two periods. The average degradation rates were determined to be 5.8% and 4.6% per year for channels 1 and 2, respectively.

The simple method given in the paper for determining the sensor degradations required that the observed albedo measurements be taken at nearly the same solar zenith angles. Therefore, the two datasets used for comparison should be sampled from the same season with consideration given to the equatorial crossing time to keep the solar zenith angles consistent. In principle, the method in this paper can be applied to the calibration and normalization of the NOAA satellites. However, to achieve a nearly real-time calibration, the method's main difficulty is how to easily establish the same sun–sensor–target geometric condition for comparison. The same problem also can be met when this method is used for the satellite normalization study since for different satellite, large differences in equatorial crossing time may exist and therefore cause the large differences in solar zenith angle. To solve this problem, other techniques such as angular parameter correction or the principle of reciprocity, which allows solar zenith angle and viewing zenith angle to be interchanged, would be helpful for the present method to be applicable.

REFERENCES

Brest, C. L., and Rossow, W. B., 1992: Radiometric calibration and monitoring of NOAA AVHRR data for ISCCP. *Int. J. Remote Sens.*, **2**, 235–273.

Gao, Z., 1989: An investigation in the Badan Jilin Desert. *Nature*, **37**, 14–17 (in Chinese).

Holben, B. N., Kaufman, Y. J., and Kendall, J. D., 1990: NOAA-11 AVHRR visible and near-IR inflight calibration. *Int. J. Remote Sens.*, **8**, 1511–1519.

Kaufman, Y. J., and Holben, B. N., 1992: Calibration of the AVHRR visible and near-IR bands by atmospheric scattering, ocean glit and desert reflection. *Int. J. Remote Sens.*, in press.

Staylor, W. F., 1990: Degradation rates of the AVHRR visible channel for the NOAA 6, 7, and 9 spacecraft. *J. Atmos. Oceanic Technol.*, **7**, 411–423.

——, and J. T. Suttles, 1986: Reflection and emission models for deserts derived from Nimbus-7 ERB scanner measurements. *J. Climate Appl. Meteor.*, **25**, 196–202.

Taylor, V. R., and L. L. Stowe, 1984: Atlas reflectance patterns for uniform earth and cloud surfaces. NOAA Tech. Rep. NESDIS 10, 66 pp.

Wu, A., 1990: Anisotropic correction of the AVHRR reflectance data over the Heihe basin. *J. Plateau Meteor.*, **9**, 136–143 (in Chinese).

——, and Q. Zhong, 1992: Seasonal variation of surface albedo and vegetation index over the Heihe experimental area. *J. Plateau Meteor.*, **11**, 440–450 (in Chinese).

Yang, Y., 1990: An investigation crossing the Takalama Desert. *Encycl. Knowledge*, **5**, 62–65 (in Chinese).